BMC Psychiatry

RESEARCH

Open Access

Cerebellar microstructural abnormalities in patients with somatic symptom disorders

Wenshuang Tang[1], Chao Zhang[2,3], Yapeng Qi[1], Qichen Zhou[1], Huazhi Li[1], Xiao-Han Shen[2,3], Lan Liu[2,3], Weikan Wang[2,3], Jian-Ren Liu[2,3*] and Xiaoxia Du[1,4*]

Abstract

Background Somatic Symptom Disorder (SSD) is a condition often linked to excessive health anxiety and somatic symptoms. In recent years, studies have found associations between the cerebellum and various mental illnesses, including SSD. However, the microstructure of cerebellar subregions in SSD using diffusion magnetic resonance imaging has not been fully defined.

Methods This is a cross-sectional study, that included 30 SSD patients and 30 age- and gender-matched healthy controls to investigate the microstructure of the cerebellum using diffusion magnetic resonance imaging. SSD diagnosis followed DSM-5 criteria, excluding major psychiatric comorbidities, while healthy controls underwent rigorous screening to exclude psychiatric or neurological histories. Clinical evaluations utilized standardized scales to assess depressive, anxiety, and cognitive symptoms. MRI data were acquired using a 3T Siemens Prisma scanner, including T1-weighted and diffusion-weighted imaging (30 directions, b = 1000/2000 s/mm^2). Multi-compartment diffusion magnetic resonance imaging metrics from free water elimination diffusion tensor imaging and neurite orientation dispersion and density imaging were used to observe microstructural changes in the cerebellum's white matter and gray matter subregions in SSD patients.

Results Compared to the control group, patients with SSD exhibited significant alterations in white matter microstructure. These changes were characterized by increased free water-eliminated fractional anisotropy and neurite density index, as well as decreased free water-eliminated mean diffusivity and radial diffusivity. Furthermore, the cerebellum displayed varying microstructural changes across 26 gray matter subregions. These changes included reduced mean diffusivity, free water-eliminated axial diffusivity, and free water-eliminated radial diffusivity, alongside increased neurite density index and orientation dispersion index. Importantly, the study identified significant correlations between these microstructural changes and clinical symptoms. Specifically, Vermis X and the left lobule VIIb showed significant associations with both depression and anxiety scores.

Conclusions The findings suggest greater neurite density and enhanced diffusion restriction in the cerebellum of patients with SSD, which may indicate possible adaptive changes associated with chronic stress.

Keywords Somatic symptom disorder, Cerebellum, Microstructure, Diffusion tensor imaging

*Correspondence:
Jian-Ren Liu
liujr021@sjtu.edu.cn
Xiaoxia Du
duxiaoxia@sus.edu.cn
[1]School of Psychology, Shanghai University of Sport, 399 Changhai Road, Yangpu District, Shanghai 200438, China
[2]Department of Neurology, Shanghai Ninth People's Hospital, Shanghai Jiao Tong University School of Medicine, 639 Zhizaoju Road, Shanghai 200011, China
[3]Clinical Research Center, Shanghai Jiao Tong University School of Medicine, Shanghai, China
[4]Center for Exercise and Brain Science, Shanghai University of Sport, Shanghai, China

Introduction

In 2013, the American Psychiatric Association introduced "somatic symptom disorder" (SSD) in DSM-5 (300.82) as a new diagnostic category, characterized by distressing somatic symptoms, excessive health-related thoughts/behaviors, and persistence over 6 months [1, 2]. General population studies using self-report questionnaires [3] found a mean SSD frequency of 12.9% [1]. SSD significantly impairs quality of life, and its pathological mechanisms remain unclear. Neuroimaging studies reveal abnormalities in brain structure and function, particularly in cognitive control, emotion regulation, stress, and somatic-visceral perception networks [4–6], with the cerebellum playing a key role in SSD pathology [7, 8].

Recent research highlights the cerebellum's expanding role in mental illness, moving beyond its traditional association with motor coordination and balance to include higher-order cognitive, emotional, and autonomic functions [9–11]. The cerebellum is now recognized as crucial in regulating motivational and emotional states, with implications for cognitive, emotional, and reward processes [9, 12, 13]. Its developmental and functional alterations are linked to neurodevelopmental disorders like autism spectrum disorder and attention deficit hyperactivity disorder [14]. Furthermore, neuroimaging studies reveal cerebellar abnormalities in psychiatric conditions such as post-traumatic stress disorder (PTSD) [15–17], schizophrenia [18, 19], depression, and anxiety [20, 21], underscoring its significance in emotion and psychiatric disorders [22].

Analyses using the Human Connectome Project dataset reveal that specific cerebellar cortex regions are involved in diverse functions, including movement, language, working memory, social interactions, and emotional regulation [23]. Motor functions primarily engage lobules IV/V/VI and VIII, while nonmotor functions involve lobule VI/Crus I, Crus II/VIIB, and lobule IX/X [23, 24]. Previous studies found abnormal cerebellar structure and function in SSD patients [7, 8], but the relationship between specific cerebellar subregion abnormalities and SSD remains unclear. Given the cerebellum's extensive functional connections with the forebrain and its regulatory role in brain functions [25, 26], we hypothesize that localized cerebellar subregion changes in SSD affect corresponding brain functions and contribute to SSD's pathological and behavioral manifestations.

High-resolution diffusion tensor imaging (DTI) and a cerebellar atlas were utilized to investigate microstructural changes in cerebellar subregions of SSD patients and their correlation with clinical symptoms. Advanced multi-compartment diffusion MRI metrics, including free water elimination DTI (FWE-DTI) [27] and neurite orientation dispersion and density imaging (NODDI) [28], were employed to assess white and gray matter microstructure in SSD patients compared to healthy controls (HCs). This approach offers significant advantages over traditional DTI: (1) FWE-DTI minimizes cerebrospinal fluid partial volume effects, enhancing structural observations in cerebellar subregions near cerebrospinal fluid [27]; (2) FWE-DTI and NODDI enable simultaneous examination of both white and gray matter microstructure, unlike conventional DTI metrics primarily suited for white matter; (3) NODDI incorporates physiological assumptions about intra/extra-neurite processes and free water compartments, providing a more biologically plausible model of tissue microstructure than standard DTI [28]. This methodological advancement allows for a more precise characterization of cerebellar abnormalities in SSD.

Methods and materials

Study design and setting

This study was a cross-sectional case-control study by retrospectively analyzing DTI data of patients with SSDs and HCs that had been collected in the past, as well as clinical scores of patients with SSDs. The aim was to investigate microstructural abnormalities in cerebellar subregions and their association with clinical symptoms (anxiety, depression, etc.) in patients with SSDs. This study involved 60 participants in total: 30 SSD patients, who were all recruited between 2018 and 2020 from Shanghai Jiao Tong University School of Medicine's 9th People's Hospital. Thirty age- and gender-matched healthy control (HC) participants were recruited through offline advertising and online recruitment. The recruitment process can be found in Supplementary Material 1.

Eligibility criteria

SSD patients were diagnosed by hospital neurologists and psychiatrists according to the DSM-5. The inclusion criteria for SSD patients were as follows: (1) age between 20 ~ 69 years; (2) right-handedness; (3) diagnosed with SSD based on DSM-5 criteria requiring two or more somatic symptoms; (4) not suffering from any other major psychiatric disorders in addition to SSD-related symptoms (Patients with minor SSD-related anxiety and depression, are not excluded). HCs were closely screened through diagnostic interviews to exclude participants with a current or past history of major illness or psychiatric illness and a family history of psychiatric illness. The following criteria were used to exclude SSD patients and HCs: (1) had a prior medical history of central nervous system disease or severe head injury; (2) is or has been suffering from another major mental illness, such as schizophrenia, bipolar disorder, mental retardation, etc.; (3) alcoholism, or met the criteria for substance abuse or dependence; (4) left-handedness; (5) having symptoms that make an MRI scan inappropriate, such

as claustrophobia. After explaining the study's goal and scanning requirements, written informed consent was obtained from each participant before participation.

Collection of clinical data

Every participant's demographic information, including age and gender, was documented. Clinical information about SSD patients, such as the primary complaint, length of sickness, and emotional state, was also reported. The Depressive Symptom Screening Scale (PHQ-9) [29], the Generalized Anxiety Self-Rating Scale (GAD-7) [30], the Hamilton Anxiety Inventory (HAMA) [31], the Hamilton Depression Scale (HAMD) [32], and the Brief Mental State Examination (MMSE) [33] were used to assess the patients' mood disorders. The PHQ-9 comprises nine items, each rated on a 4-point Likert scale ranging from 0 ("not at all") to 3 ("nearly every day"). The total score ranges from 0 to 27, with a score of ≥10 typically indicating moderate depressive symptoms and a score of ≥20 suggesting severe depression. Similarly, the GAD-7 consists of seven items, also scored on a 4-point scale from 0 ("not at all") to 3 ("nearly every day"). The total score ranges from 0 to 21, with scores of 5, 10, and 15 generally representing mild, moderate, and severe anxiety symptoms, respectively. The HAMA includes 14 items, each rated based on symptom severity on a scale from 0 to 4. The total score ranges from 0 to 56, with a score of ≥17 typically indicating clinically significant anxiety symptoms. The HAMD consists of 17 items, each scored on a scale from 0 to 4 based on symptom severity. The total score ranges from 0 to 52, with scores of ≥7 indicating mild depressive symptoms, ≥20 indicating moderate depression, and ≥30 suggesting severe depression. The MMSE evaluates cognitive functions, including orientation to time and place, memory, attention, language, and visuospatial abilities. The total possible score is 30, with scores below 24 potentially indicating cognitive impairment.

MRI data acquisition

All MRI data were acquired on a 3 Tesla Siemens Prisma system using a 64-channel head coil. Three-dimensional, high-resolution T_1-weighted whole-brain images were obtained utilizing magnetization-prepared rapid-acquisition gradient-echo sequences. The parameters were defined as follows: image resolution of $1 \times 1 \times 1$ mm^3; repetition time of 2.53 s; echo time of 2.34 s; inversion time of 1.1 s; and a flip angle of 7 degrees. In addition, to exclude participants with abnormal white matter changes, whole-brain T2-weighted images were also acquired in this study.

All participants covered the entire brain for the scans performed. A diffusion-weighted spin-echo echo-planar imaging sequence acquired MR diffusion data in 30 directions at two b values (b = 1000 s/mm² and b = 2000 s/mm²), and 10 non-diffusion-weighted images (b = 0 s/mm²) were also acquired. The data acquisitions were accelerated using parallel imaging with a factor of 4. Seventy-four consecutive slices were generated in the brain using the following parameters: isotropic voxel size of $2 \times 2 \times 2$ mm^3, repetition time of 5 s, and echo time of 95 ms.

MRI data analysis

FMRIB Software Library (FSL version 5.0, http://fsl.fmrib.ox.ac.uk) was used to process the MRI data. Pre-processing was performed with FSL, including data quality checking and format conversion, head motion artifacts and eddy current distortions, gradient directions correction, and removal of non-cerebral tissue to obtain a brain mask. After gathering pre-processed data from each participant, the analysis moved on to the next step.

FWE-DTI analysis

FWE-DTI was performed by fitting the signal S_i[34]

$$S_i = S_0[f\ exp\,(-bD_{iso}) + (1-f)\exp(-bg_i^T Dg_i\,)]$$

In the above equation, $S_0$is the signal from the non-diffusion-weighted (b = 0) volumes,

f is the volume fraction of free water contamination, b is the diffusion weight (i.e., the b-value), D_{iso} is the isotropic diffusion coefficient of free water, which is set to be 3.0×10^{-3} mm^2/s, g_i is the direction of the diffusion gradient, and D is the diffusion tensor of the tissue. The free water parameters are f and D, where the characteristic decomposition of D yields DTI metrics (indicated by a 't' suffix, i.e., FAt, MDt, ADt, RDt) [27]. In this study, the free water exclusion diffusion tensor model of dipy software [35]. The preprocessed data was utilized to fit the model, calculate the FWE-DTI metrics, and derive the free water index (FAt, MDt, ADt, RDt, FW).

NODDI analysis

NODDI is based on a three-compartment tissue, which assumes the presence of three different types of movement-restricting water molecules in each pixel: glial cells, axons, and extra-cellular space [28]. It categorizes the microstructural environment into three distinct compartments: intracellular, extracellular, and cerebrospinal fluid compartments. Each compartment significantly influences water diffusion within the environment [36] and generates a distinct normalized MR signal. The complete normalized signal A can be expressed as [28]:

$$A = (1 - v_{iso})\,(v_{ic}A_{ic} + (1 - v_{ic})\,A_{ec}) + v_{iso}A_{iso}$$

The variables A_{ic} and v_{ic} represent the normalized signal and volume fraction of the intracellular compartment, respectively. The variable A_{ec}indicates the normalized signal of the extracellular compartment. Additionally, A_{iso} and v_{iso} correspond to the normalized signal and volume fraction of the cerebrospinal fluid compartment, respectively. In this study, AMICO software [37] was used to estimate NODDI indicators, accelerate the fitting speed of the NODDI model without affecting the significance, and calculate and derive NODDI metrics: free water fraction (FWF), orientation dispersion index (ODI), neurite density index (NDI).

Extraction of mean signal values from cerebellar ROIs

ROI-averaged signals were also extracted in the FSL. Firstly, all the metrics of FWE-DTI and NODDI derived above were aligned to the standard space using the FNIRT tool, using linear and nonlinear alignment, respectively. Secondly, the average image and white matter skeleton were constructed based on all the metrics aligned to the standard space. Next, based on the cerebellar SUIT template that has been aligned to standard space [38, 39], the Johns Hopkins University White Matter Structural Atlas [40–42], the fslmaths tool was used to extract the gray matter brain ROIs in the cerebellum (the extracted brain regions included: lobules I-IV; the left and right lobules V; the left and vermis lobules Crus I; the left, vermis and right lobules VI, Crus II, VIIb, VIIIa, VIIIb, IX, and X), and extracted white matter brain ROIs in the cerebellum (extracted brain regions: left and right superior cerebellar peduncle, middle cerebellar peduncle, and left and right inferior cerebellar peduncle). Finally, the average signal values of the cerebellar ROIs for the corresponding metrics were extracted using the fslmeants tool.

Statistical analysis

SPSS statistical software (version 26.0, IBM, Armonk, NY, USA) assessed the differences between SSD patients and HCs. The Shapiro-Wilk test was used to assess the normality of the data. In contrast, the demographic data were analyzed using independent samples t-test and chi-square test for continuous and categorical variables, respectively. The statistical significance of all two-sided tests was set at 0.05. A general linear model was applied for the ROIs signal values of FWE-DTI and NODDI metrics between-group comparisons, with age and gender as covariates. To control for false positives due to multiple comparisons, we conducted false discovery rate (FDR) correction on the *p*-values of all metrics, grouped by 26 different cerebellar subregions, and performed a total of 8 such corrections. The corrected *p*-values were used to determine statistical significance, with a significance level set at $p < 0.05$ after correction.

Table 1 Demography and clinical scores of the SSDs group and HCs group

	SSD group	HC group	*p*-value
Gender (F, M)	17, 13	18, 12	0.79
Age (year)	53.50 ± 9.46	53.50 ± 9.72	1.00
Disease duration (months)	39.67 ± 5.48	-	
PHQ-9	7.40 ± 0.85	-	
GAD-7	6.77 ± 0.87	-	
HAMA	9.63 ± 0.86	-	
HAMD	9.57 ± 1.07	-	
MMSE	27.38 ± 0.24	-	

Data are presented as numbers, mean ± SD. SSD, somatic symptom disorders; PHQ-9, Patient Health Questionnaire; GAD-7, Generalized Anxiety Disorder; HAMA, Hamilton Anxiety Scale; HAMD, Hamilton Depression Scale; MMSE, Minimum Mental State Examination;-, no data

Correlation analysis

The mean signal values of different cerebellar regions of FAt, MDt, ADt, RDt, FW, FWF, ODI, and NDI extracted from SSD patients were correlated with clinical data. Expectation maximization method, an iterative algorithm based on great likelihood estimation, was used to fill in the missing values of the clinical data to improve the completeness of the data and to reduce the bias due to missing data. The ROIs signal values and the clinical score (i.e., PHQ-9, GAD-7, HAMA, HAMD, and MMSE scores) were analyzed by bivariate Pearson correlation. To control for false-positive results due to multiple comparisons, we applied false FDR correction to the *p*-values that were significant at the 0.05 level. These *p*-values were grouped according to five different clinical scores for the same brain regions and indicators, resulting in a total of 19 groups, with a total of 95 comparisons. The corrected *p*-values were used to determine statistical significance.

Results

Patients with SSDs included 17 females and 13 males, age: 53.50 ± 9.46; HCs included 18 females and 12 males, age: 53.50 ± 9.72. The age ($t = 0.000$, $p = 1.000$) and sex ($\chi^2 = 0.069$, $p = 0.793$) distributions of SSD patients and HCs did not differ significantly. Among the SSD patients, 14 complained of headaches, dizziness, or other symptoms, and 16 complained of localized body numbness or other physical discomfort. All SSDs were either in mild anxiety or depression except for individual patients who had no symptoms of depression and anxiety. Cognition was normal in all patients. Table 1 displays the participants' clinical scores and demographic information.

Cerebellar white matter microstructure based on white matter atlas

Based on the white matter atlas from Johns Hopkins University, compared with HCs, patients with SSDs exhibited significantly increased FAt in the SCP, MCP, and ICP. Except for the left SCP, NDI was significantly increased

in all subregions, RDt was significantly decreased in all subregions (Table 2; Fig. 1). Additionally, MDt was significantly decreased in the right SCP and the MCP. The right ICP showed significant decreases in FW (Table 2; Fig. 1). For more detailed information regarding these results, please refer to Supplementary Material 2 stable1. The supplementary material includes comprehensive statistical analyses, such as *p*-values, effect sizes, and 95% confidence intervals (CIs) for all reported findings.

Microstructure of cerebellar gray matter subregion based on SUIT template

With age and gender as covariates and considering a significant group difference with FDR-corrected $p<0.05$ as the criterion, the following findings were observed based on the SUIT template for cerebellar parcellation. Compared with HCs, individuals with SSDs exhibited significantly decreased MDt in all cerebellar gray matter subregions except for the right lobules I–IV, Crus II, VIIb, VIIIb, and the vermis and right side of lobule X (Table 2). RDt values showed significant decreases in the same regions as MDt, with additional significant reductions in lobules I–IV. ADt values were significantly

Table 2 FWE-DTI and NODDI metrics changes in cerebellar regions in somatic symptom disorders

Region	FWE-DTI parameters					NODDI parameters		
	FAt	MDt (mm^2/s)	ADt (mm^2/s)	RDt (mm^2/s)	FW	FWF	ODI	NDI
White matter (JHU-WM labels)								
Left SCP	↑	-	-	-	-	-	-	-
Right SCP	↑	↓	-	↓	-	-	-	↑
MCP	↑	↓	-	↓	-	-	-	↑
Left ICP	↑	-	-	↓	-	-	-	↑
Right ICP	↑	-	-	↓	↓	-	-	↑
Gray matter (SUIT)								
I-IV	-	-	-	↓	-	-	-	↑
Left V	-	↓	-	↓	-	-	-	↑
Right V	-	↓	↓	↓	-	-	-	↑
Left VI	-	↓	↓	↓	-	-	-	↑
Vermis VI	-	↓	↓	↓	-	-	↑	↑
Right VI	-	↓	↓	↓	↓	-	↑	↑
Left Crus I	-	↓	↓	↓	↓	-	-	↑
Vermis Crus I	-	↓	-	↓	-	-	↑	↑
Left Crus II	-	↓	↓	↓	↓	-	↑	↑
Vermis Crus II	-	↓	↓	↓	-	-	↑	↑
Right CrusII	-	-	-	-	-	-	-	↑
Left VIIb	-	↓	↓	↓	-	-	-	↑
Vermis VIIb	-	↓	↓	↓	-	-	-	↑
Right VIIb	-	-	↓	-	-	-	-	↑
Left VIIIa	-	↓	↓	↓	-	-	-	↑
Vermis VIIIa	-	↓	↓	↓	-	-	-	↑
Right VIIIa	-	↓	↓	↓	-	-	-	↑
Left VIIIb	-	↓	-	↓	-	-	-	↑
Vermis VIIIb	-	↓	↓	↓	-	-	-	↑
Right VIIIb	-	-	-	-	-	-	-	↑
Left IX	-	↓	-	↓	-	-	-	↑
Vermis IX	-	↓	↓	↓	-	-	-	↑
Right IX	-	↓	↓	↓	-	-	↑	↑
Left X	-	↓	-	↓	-	-	-	↑
Vermis X	-	-	-	-	-	-	-	↑
Right X	-	-	-	-	-	-	-	↑

Arrows indicate increases or decreases in corresponding parameters in cerebellar-related regions in SSD patients compared with healthy controls. FWE-DTI, free water elimination diffusion tensor imaging; NODDI, neurite orientation dispersion, and density imaging; SCP, superior cerebellar peduncle; MCP, middle cerebellar peduncle; ICP, inferior cerebellar peduncle; FAt, free water elimination fractional anisotropy; MDt, free water elimination mean diffusivity; ADt, free water elimination axial diffusivity; RDt, free water elimination radial diffusivity; FW, free water; FWF, free water fraction; ODI, orientation dispersion index; NDI, neurite density index; ↑, controlling for age and gender as a covariate, the signal value of this indicator was significantly higher in SSD patients ($p<0.05$). ↓, controlling for age and gender as a covariate, the signal value of this indicator was significantly lower in SSD patients ($p<0.05$). -, No significant change. The *p*-values for both white and grey matter were parametrically corrected for FDR

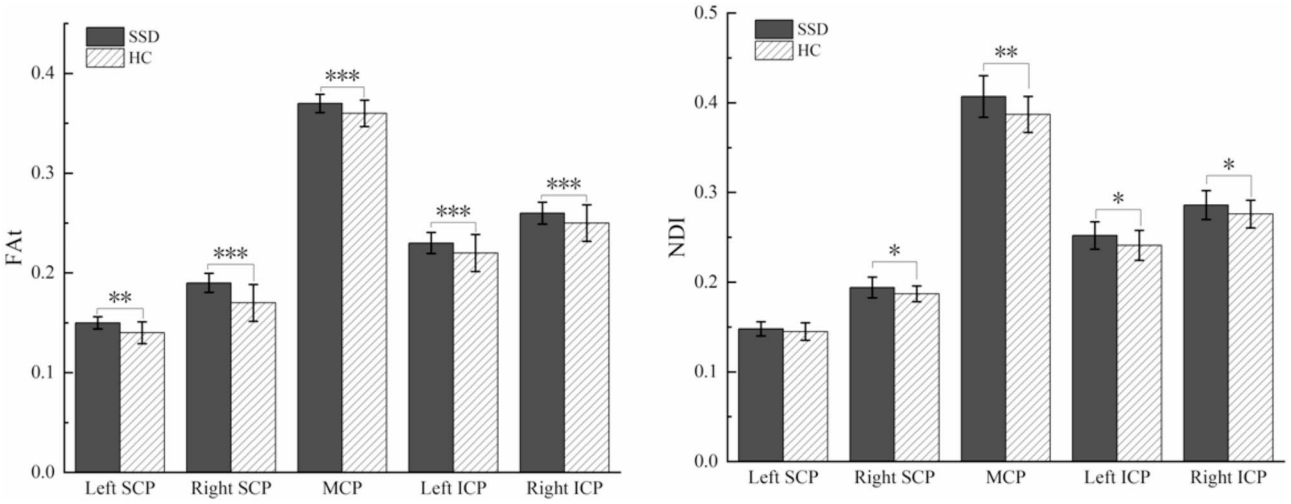

Fig. 1 FWE-DTI and NODDI metrics changes in cerebellar white matter tract in somatic symptom disorders. FWE-DTI, free water elimination diffusion tensor imaging; NODDI, neurite orientation dispersion, and density imaging; SCP, superior cerebellar peduncle; MCP, middle cerebellar peduncle; ICP, inferior cerebellar peduncle; FAt, free water elimination fractional anisotropy; NDI, neurite density index; *, indicates statistically significant group comparisons with $P < 0.05$; **, indicates statistically significant group comparisons with $P < 0.01$; ***, indicates statistically significant group comparisons with $P < 0.001$

decreased in the right side of lobule V, lobule VI, the left side and vermis of Crus I, the left side, and vermis of Crus II, the vermis and right side of lobule VIIb, the vermis of lobule VIIIa, the vermis and right side of lobule VIIIb, and the vermis and right side of lobule IX (Table 2). FW values were significantly decreased on the right side of lobule VI, the left side of Crus I, and the left side of Crus II (Table 2). ODI values were significantly increased in the vermis and right side of lobule VI, Crus II, and the right side of lobule IX (Table 2; Fig. 2). NDI values were significantly increased across the entire cerebellar region (Table 2; Fig. 2). No significant changes were observed in FAt or FWF in the cerebellar gray matter (Table 2). For details, see Supplementary Material 2 stable2 (includes *p*-values, effect sizes, 95% CIs).

Correlation with clinical scores

FAt, FW, ODI, and FWF values in cerebellar lobules I-IV, Crus II, VIIb, VIIIa, IX, and X were significantly correlated ($p < 0.05$ uncorrected) with clinical data. However, no significant correlation was found between MDt, ADt, RDt, NDI, and clinical data in all cerebellar regions. More details are in Table 3.

After applying the FDR correction, the diffusion metrics of the left lobule VIIb of the cerebellum demonstrated robust and statistically significant correlations with various clinical measures. Specifically, FAt exhibited a significant negative correlation with the GAD-7 score (r = -0.502, $p = 0.025$). In contrast, FW showed significant positive correlations with the HAMA ($r = 0.412$, $p = 0.040$), the HMAD ($r = 0.507$, $p = 0.013$), and the MMSE ($r = 0.497$, $p = 0.013$). Additionally, the FWF was significantly positively correlated with the PHQ-9 ($r = 0.400$, $p = 0.047$), HAMA ($r = 0.496$, $p = 0.020$), and HMAD ($r = 0.475$, $p = 0.020$).

Furthermore, the FAt of the vermis of lobule X in the cerebellum also revealed significant negative correlations with multiple clinical measures, including PHQ-9 (r = -0.435, $p = 0.016$), GAD-7 (r = -0.405, $p = 0.027$), HAMA (r = -0.480, $p = 0.024$), and HMAD (r = -0.464, $p = 0.024$). These findings suggest that microstructural alterations in specific cerebellar regions, as indicated by diffusion metrics, are closely associated with variations in anxiety, depression, and cognitive function, even after stringent correction for multiple comparisons.

Discussion

This study identified significant microstructural alterations in both white matter and gray matter of the cerebellum in patients with SSDs. In white matter, SSD patients exhibited increased FAt, decreased MDt and RDt, and elevated NDI, particularly in the bilateral SCP, ICP, and MCP. In gray matter, microstructural changes were observed across 26 subregions, characterized by reduced MDt, ADt, RDt, FW, and FWF, alongside increased NDI and ODI. These findings suggest enhanced neurite density and diffusion restriction in the cerebellum of SSD patients, potentially reflecting adaptive neuroplastic responses to chronic stress [43]. Notably, alterations in the left lobule VIIb of the cerebellum were significantly correlated with clinical symptoms of depression and anxiety, underscoring the cerebellum's involvement in SSD pathophysiology. These results highlight the cerebellum as a potential therapeutic target for modulating neural plasticity and mitigating associated psychiatric symptoms in SSDs.

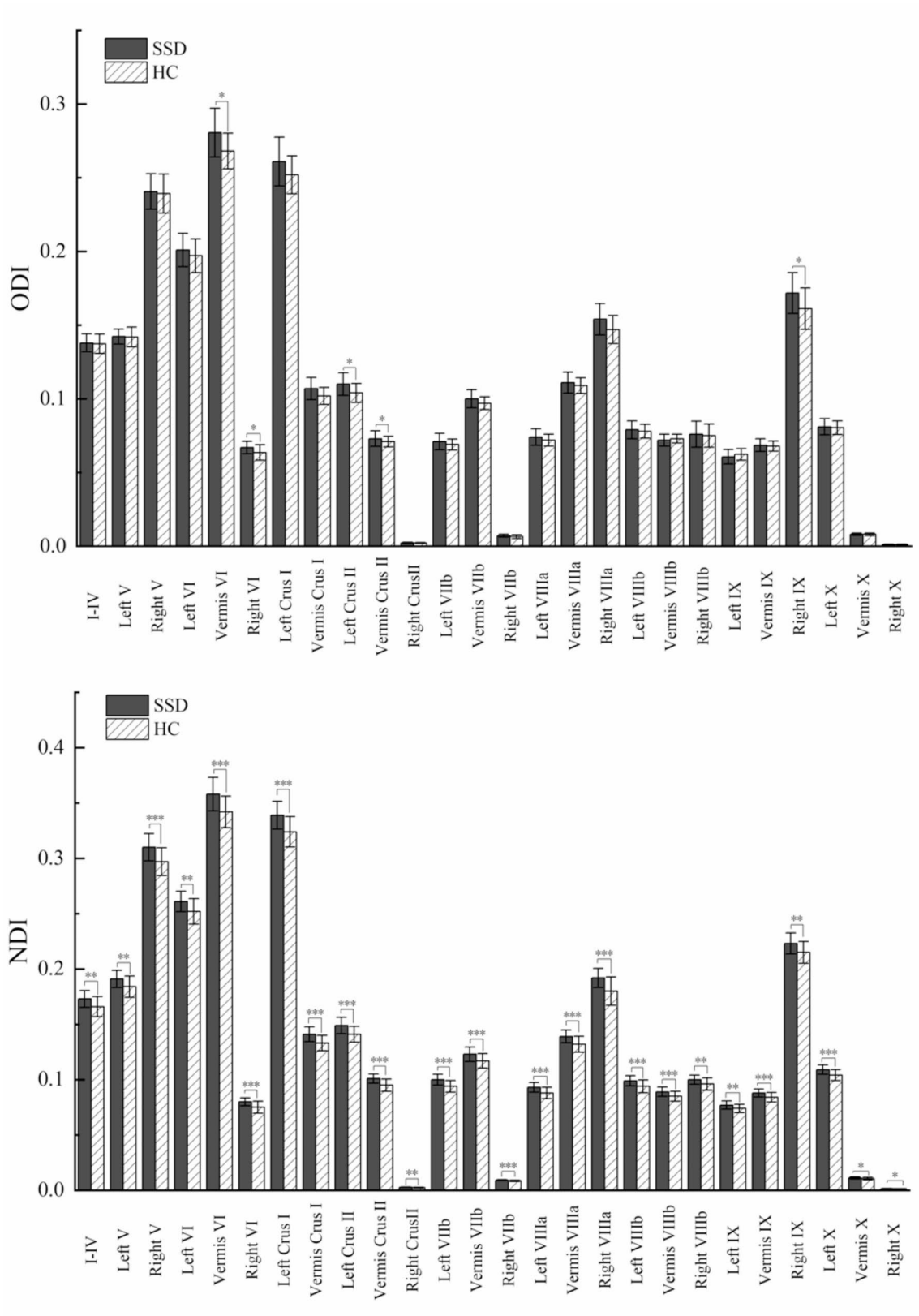

Fig. 2 Changes in NODDI metrics in cerebellar gray matter subregions in patients with somatic symptom disorders and healthy controls. NODDI, neurite orientation dispersion and density imaging; ODI, orientation dispersion index; NDI, neurite density index; *, indicates statistically significant group comparisons with $P < 0.05$; **, indicates statistically significant group comparisons with $P < 0.01$; ***, indicates statistically significant group comparisons with $P < 0.001$

Table 3 Correlation between diffusion parameters in the cerebellum and emotions

	I-IV	Left CruosII	Right CrusII	Left VIIb	Vermis VIIb	Vermis VIIIa	Right VIIIa	Right VIIIb	Right IX	Left X	Vermis X	Right X
FAt												
PHQ-9	−0.161	−0.340	−0.270	−0.321	**−0.426***	**−0.450***	**−0.404***	−0.242	−0.003	−0.071	**−0.435****	0.252
GAD-7	−0.275	−0.309	**−0.440***	**−0.502****	**−0.402***	**−0.393***	**−0.405***	−0.203	−0.081	−0.018	**−0.405****	0.281
HAMA	−0.189	−0.226	−0.358	**−0.363***	−0.361	**−0.377***	−0.350	−0.224	−0.134	0.014	**−0.480****	0.186
HMAD	−0.163	−0.216	-,321	**−0.366***	**−0.377***	−0.357	−0.343	−0.182	−0.125	−0.016	**−0.464****	0.208
MMSE	0.002	−0.015	−0.054	0.029	0.155	0.121	0.183	**0.434***	**0.368***	**0.381***	0.093	0.254
FW												
PHQ-9	0.046	0.335	0.080	**0.374***	0.180	0.178	0.254	0.311	0.226	0.343	0.003	−0.040
GAD-7	0.023	0.296	0.102	**0.412****	0.148	0.054	0.187	0.245	0.207	0.197	0.078	−0.054
HAMA	0.114	**0.415***	0.205	**0.507****	0.190	0.118	0.215	0.301	0.237	0.235	0.052	0.014
HMAD	0.120	**0.422***	0.146	**0.497****	0.213	0.112	0.203	0.288	0.304	0.198	0.054	0.065
MMSE	0.095	−0.225	−0.157	−0.213	−0.211	−0.176	−0.092	0.038	−0.119	−0.177	0.191	**−0.407***
ODI												
PHQ-9	0.319	0.138	0.028	0.051	0.282	0.289	0.338	**0.388***	0.213	0.123	**0.458***	−0.229
GAD-7	**0.386***	0.108	0.048	0.125	0.230	0.279	0.319	0.276	0.260	−0.010	**0.392***	−0.335
FWF												
PHQ-9	0.097	0.332	0.070	**0.400****	0.126	0.139	0.209	**0.373***	0.261	0.344	−0.029	−0.010
HAMA	0.137	**0.415***	0.194	**0.496****	0.167	0.111	0.157	0.342	0.240	0.209	0.025	0.027
HMAD	0.150	**0.405***	0.151	**0.475****	0.182	0.118	0.144	0.339	0.308	0.177	0.024	−0.083
MMSE	0.077	−0.091	−0.139	−0.028	−0.246	−0.194	−0.040	−0.025	−0.134	−0.193	0.197	**−0.430***

Significant correlations have been highlighted in bold. FAt, free water elimination fractional anisotropy; FW, free water; ODI, orientation dispersion index; FWF, free water fraction; PHQ-9, Patient Health Questionnaire-9; GAD-7, Generalized Anxiety Disorder-7; HAMA, Hamilton Anxiety Rating Scale; HMAD, Hamilton Mood and Anxiety Disorders Scale; MMSE, Minimum Mental State Examination; *, $p < 0.05$, uncorrected; **, $p < 0.05$, FDR corrected

DTI is a highly sensitive imaging modality capable of detecting subtle microstructural changes in the brain. By employing advanced diffusion models, such as DTI-FWE and NODDI, this study extracted detailed microstructural information that surpasses the limitations of traditional single-compartment diffusion metrics. DTI-FWE utilizes a dual tensor model to differentiate intracellular and extracellular free water diffusion, enabling a more precise assessment of tissue microstructure [44]. NODDI, on the other hand, provides specific estimates of neurite density and orientation dispersion, offering deeper insights into the factors contributing to fractional anisotropy [28]. By integrating DTI-FWE and NODDI parameters, this study elucidated the microstructural and physiological changes associated with SSDs, providing a comprehensive understanding of the disorder's neurobiological underpinnings.

According to the White Matter Structural Atlas analyses, SSD patients demonstrate greater diffusion restriction (i.e., higher FAt/NDI, lower MDt/RDt) in the white matter tract than HCs. The cerebellum is a brain region that is sensitive to stress, and previous literature has found that the cerebellum changes in both animals and humans after experiencing stress [43]. A comprehensive meta-analysis has demonstrated that individuals with PTSD display significantly elevated FA in the inferior frontal-occipital fasciculus and the left inferior temporal gyrus [45]. Extremely stressful life experiences that lead to PTSD are associated with significant changes in the brain's white matter network at global, nodal, and modular levels [46]. RD indicates the level of isotropic diffusion in brain tissue, measured perpendicular to maximal diffusion direction, and NDI reflects the density of neurites, including axons and dendrites, based on intracellular diffusion [47]. NDI is sensitive to age-related differences in the developing brain; neurite density is known to increase with development, and NDI was found to increase with age [48]. Thus, we speculate that SSD patients have more neurite density in the cerebellar white matter, leading to an increase in RDt, a decrease in MDt, and an increase in FAt. The elevation of NDI may indicate that in SSDs, cerebellar white matter changes neuroplasticity under stress [43].

Similar changes seem to occur in the gray matter of the cerebellum, manifested as widespread greater diffusion restriction (i.e., higher NDI/ODI, lower MDt/ADt/RDt) in gray matter than HCs.ADt indicates the degree of isotropic diffusion in brain tissue along the direction of maximum diffusion, while ODI reflects the distribution of neurites (axons and dendrites) in the intracellular compartment [47]. The increase in NDI/ODI may directly lead to a decrease in MDt/ADt/RDt, and the change in NDI/ODI may be the leading cause of microstructural changes. The decrease of NDI/ODI in gray matter is often observed in degenerative diseases, while the increase of NDI/ODI is often related to brain development [49]. The cerebellum is linked to stress-related brain regions, and many studies indicate that it responds to stress, connecting it to stress-related psychopathologies [43]. Previous literature indicates that adverse childhood experiences linked to higher NDI values are clinically significant in the pathophysiology of PTSD symptoms in individuals with autism spectrum disorder [50]. Baek et al. results indicated that the tegmental area projecting cerebellar neurons proactively regulates the development of depression-like behavior [21]. The elevation of NDI/ODI in SSD patients suggests some pathological changes in the cerebellum, which may be related to compensatory or adaptive changes in the cerebellum. Research indicates that acute and repeated stress exposure in animals impacts the cerebellum, and stressful experiences also alter cerebellar activity and structure in humans [43]. SSD patients suffer from long-term psychological stress accompanied by changes in cerebellar structural adaptability.

More and more evidence supports the role of the cerebellum in the pathophysiology of psychiatric disorders and neurodevelopmental disorders [14]. Although there are extensive cerebellar microstructural changes in SSD, more severe microstructural changes occur locally in the cerebellum. Especially in the right VI, left Crus I, and Crus II regions, additional decreases in FW and FWF indicate a decrease in extracellular space and more severe microstructural changes. The VI, Crus I, and Crus II are the core regions of cerebellar cognitive/affective first and second representations, while VI is also the first representation of motor [23, 24]. Cerebellum proposal plays a key role in regulating emotion [9]. A meta-analysis showed that the Crus II cerebellum is specialized for social mentalizing and emotional self-experiences [51]. According to the dysmetria of thought theory, the cerebellum enhances the accuracy, consistency, and appropriateness of cognitive and emotional functions, just as it does for motor-related tasks [9, 25, 26]. We speculate the microstructural changes in the cerebellum of SSD include both motor and emotional representations of the cerebellum, which may be due to function abnormalities in somatic sensation and emotional regulation in SSD patients [9, 25, 26].

Correlation analysis revealed significant associations between the microstructure of cerebellar subregions and the somatic symptoms and emotional scores of patients with SSD, with SSD-related symptoms predominantly localized in the secondary representation areas of cerebellar motor function and the secondary and third representation areas of non-motor functions, such as cognition and emotion, which are believed to be involved in higher-order regulatory processes [23, 24]. Specifically, lobule VIII, corresponding to the secondary motor

representation area, demonstrated mild correlations with the PHQ-9, GAD-7, and HAMA, suggesting a potential link to physical discomfort, while lobules VIII and IX/X, encompassing both secondary motor and third cognitive representation areas, showed mild correlations with the MMSE, implicating these regions in cognitive processing. Furthermore, the left lobule VIIb and vermis X, associated with secondary cognitive representation and third non-motor (cognition and emotion) representation, exhibited strong correlations with HAMA, HMAD, and PHQ-9 scores, highlighting their critical role in emotional regulation and cognitive-affective processing. Damage to distinct cerebellar subregions can lead to diverse functional impairments and clinical symptoms, such as cerebellar cognitive affective syndrome resulting from cognitive-limbic region impairment [25], while structural alterations in cerebellar subregions, frequently observed in psychiatric disorders like PTSD and schizophrenia spectrum disorder, are characterized by reduced cerebellar volumes in regions such as lobule VIIB, Crus II, vermis (VI, VIII), lobule X, and the corpus medullare [17, 52]. Given the cerebellum's role in predictive processing, structural abnormalities may disrupt predictive mechanisms, leading to an overestimation of negative outcomes in challenging situations and exacerbating negative emotional states such as anxiety and depression [20, 53]., underscoring the importance of cerebellar microstructure in the pathophysiology of SSD and related psychiatric conditions.

This study has several limitations that should be acknowledged. Firstly, although various diffusion MRI parameters detected microstructural changes in the cerebellum of patients with SSD, the specific physiological and pathological mechanisms underlying these alterations remain unclear. For instance, the observed increases in NDI and ODI suggest unusual microstructural reorganization, but their exact biological significance requires further investigation. Secondly, this is a cross-sectional study, which limits our ability to infer causal relationships or longitudinal changes. It remains unknown whether these cerebellar microstructural alterations in SSD patients have persisted since childhood or represent transient changes associated with the current state of the disorder. Additionally, the relatively small sample size of 30 SSD patients and 30 healthy controls may limit the generalizability of the findings and reduce the statistical power to detect subtle effects. Future studies with larger cohorts are needed to validate these results and explore potential subgroup differences. Furthermore, the study did not adjust for potential confounding variables, such as medication use, comorbidities, or lifestyle factors, which could influence cerebellar microstructure. The inability to account for these confounders represents a significant methodological limitation and should be addressed in future research. Despite these limitations, this study provides valuable preliminary insights into the cerebellar microstructural changes associated with SSD, laying the groundwork for more comprehensive investigations.

In summary, this study found that there are extensive microstructural changes in the white matter fiber bundles and subregions of cerebellar gray matter in SSD patients, with SSD patients exhibiting higher density of neural processes and greater diffusion restriction in the cerebellum, which may indicate adaptive changes due to chronic stress. We speculate that the microstructural changes in the cerebellum of SSD include both motor and non-motor representations of the cerebellum, possibly due to function abnormalities in somatic sensation and emotional regulation in SSD patients. The exact physiological mechanisms underlying the microstructural changes in the cerebellum of SSD require further research.

Abbreviations

SSDs	Somatic symptom disorders
MRI	Magnetic resonance imaging
FWE-DTI	Free water elimination diffusion tensor imaging
NODDI	Neurite orientation dispersion and density imaging
FAt	Free water eliminated fractional anisotropy
MDt	Free water eliminated mean diffusivity
RDt	Free water eliminated radial diffusivity
ADt	Free water eliminated axial diffusivity
FW	Free water
DSM-5	Diagnostic and statistical manual of mental disorders, fifth edition
PSTD	Post-traumatic stress disorder
DTI	Diffusion tension imaging
HCs	Healthy controls
PHQ-9	Depressive symptom screening scale
GAD-7	Generalized anxiety self-rating scale
HAMA	Hamilton anxiety inventory
HAMD	Hamilton depression scale
MMSE	Brief mental state examination
FSL	FMRIB software library
FWF	Free water fraction
ODI	Orientation dispersion index
NDI	Neurite density index
ROIs	Regions of interest
SUIT	Spatially unbiased infratentorial template
FDR	False discovery rate
SCP	Superior cerebellar peduncle
MCP	Middle cerebellar peduncle
ICP	Inferior cerebellar peduncle
CIs	Confidence intervals

Supplementary Information

The online version contains supplementary material available at https://doi.org/10.1186/s12888-025-06642-5.

Supplementary Material 1

Supplementary Material 2

Acknowledgements

No.

Author contributions

C. Z., X. S., LL, and W.W. collected the data, and W. T., Y. Q., Q. Z., H. L., and X. D. analyzed the data, and W. T., Y. Q., and X. D. prepared Figs. 1 and 2. All authors reviewed the manuscript.

Funding
This research was supported by grants from the Ministry of Education's Social Sciences and Humanities project (grant number 23A10277004 awarded to X. X. Du), the Shanghai Municipal Education Commission-Gaofeng Clinical Medicine Grant Support (grant number 20161422 awarded to J. R. Liu), and the Natural Science Foundation Project funded by the Shanghai Municipal Science and Technology Commission (grant number 22ZR1436900 awarded to J. R. Liu).

Data availability
The datasets generated during and/or analyzed during the current study are available from the corresponding author upon reasonable request.

Declarations

Ethics approval and consent to participate
The Human Research Committee of East China Normal University (No. HR062-2018), the Ethics Committee of Shanghai University of Sport (No. 102772024RT133), and the Ethics Committee of Shanghai Jiao Tong University School of Medicine's 9th People's Hospital (No. 2016-44-T1) all approved the study according to the principles of the Declaration of Helsinki. The written informed consent was obtained from the participants.

Consent for publication
Not applicable.

Competing interests
The authors declare no competing interests.

Received: 1 November 2024 / Accepted: 20 February 2025
Published online: 04 March 2025

References

1. Löwe B, Levenson J, Depping M, Hüsing P, Kohlmann S, Lehmann M, et al. Somatic symptom disorder: a scoping review on the empirical evidence of a new diagnosis. Psychol Med. 2022;52:632–48.
2. American Psychiatric Association. American Psychiatric Association. Diagnostic and statistical manual of mental disorders. 5th ed. 2013.
3. Demetriou C, Özer B, Essau C. Self-Report Questionnaires. 2015.
4. Kim SM, Hong JS, Min KJ, Han DH. Brain functional connectivity in patients with somatic symptom disorder. Psychosom Med. 2019;81:313–8.
5. Rossetti MG, Delvecchio G, Calati R, Perlini C, Bellani M, Brambilla P. Structural neuroimaging of somatoform disorders: A systematic review. Neurosci Biobehav Rev. 2021;122:66–78.
6. Park B, Lee S, Jang Y, Park HY. Affective dysfunction mediates the link between neuroimmune markers and the default mode network functional connectivity, and the somatic symptoms in somatic symptom disorder. Brain Behav Immun. 2024;118:90–100.
7. Liang H-B, Dong L, Cui Y, Wu J, Tang W, Du X, et al. Significant structural alterations and functional connectivity alterations of cerebellar Gray matter in patients with somatic symptom disorder. Front Neurosci. 2022;16:816435.
8. Dong L, Liang H-B, Du J, Wang Y, Zhou Q, Xin Z, et al. Microstructural differences of the Cerebellum-Thalamus-Basal Ganglia-Limbic cortex in patients with somatic symptom disorders: a diffusion kurtosis imaging study. Cerebellum. 2023;22:840–51.
9. Strata P. The emotional cerebellum. Cerebellum. 2015;14:570–7.
10. King M, Hernandez-Castillo CR, Poldrack RA, Ivry RB, Diedrichsen J. Functional boundaries in the human cerebellum revealed by a multi-domain task battery. Nat Neurosci. 2019;22:1371–8.
11. Stoodley CJ, Schmahmann JD. Functional topography of the human cerebellum. Handb Clin Neurol. 2018;154:59–70.
12. Rudolph S, Badura A, Lutzu S, Pathak SS, Thieme A, Verpeut JL, et al. Cognitive-Affective functions of the cerebellum. J Neurosci. 2023;43:7554–64.
13. Schutter DJLG. The cerebellum and disorders of emotion. Adv Exp Med Biol. 2022;1378:273–83.
14. Stoodley CJ. The cerebellum and neurodevelopmental disorders. Cerebellum. 2016;15:34–7.
15. He H, Luo C, Luo Y, Duan M, Yi Q, Biswal BB, et al. Reduction in Gray matter of cerebellum in schizophrenia and its influence on static and dynamic connectivity. Hum Brain Mapp. 2019;40:517–28.
16. Killion BE, Weyandt LL. Brain structure in childhood maltreatment-related PTSD across the lifespan: A systematic review. Appl Neuropsychol Child. 2020;9:68–82.
17. Huggins AA, Baird CL, Briggs M, Laskowitz S, Hussain A, Fouda S, et al. Smaller total and subregional cerebellar volumes in posttraumatic stress disorder: a mega-analysis by the ENIGMA-PGC PTSD workgroup. Mol Psychiatry. 2024;29:611–23.
18. Zhuo C, Wang C, Wang L, Guo X, Xu Q, Liu Y, et al. Altered resting-state functional connectivity of the cerebellum in schizophrenia. Brain Imaging Behav. 2018;12:383–9.
19. Brady RO, Gonsalvez I, Lee I, Öngür D, Seidman LJ, Schmahmann JD, et al. Cerebellar-Prefrontal network connectivity and negative symptoms in schizophrenia. Am J Psychiatry. 2019;176:512–20.
20. Moreno-Rius J. The cerebellum in fear and anxiety-related disorders. Prog Neuropsychopharmacol Biol Psychiatry. 2018;85:23–32.
21. Baek SJ, Park JS, Kim J, Yamamoto Y, Tanaka-Yamamoto K. VTA-projecting cerebellar neurons mediate stress-dependent depression-like behaviors. eLife. 2022;11:e72981.
22. Shakiba A. The role of the cerebellum in neurobiology of psychiatric disorders. Neurol Clin. 2014;32:1105–15.
23. Guell X, Gabrieli JDE, Schmahmann JD. Triple representation of Language, working memory, social and emotion processing in the cerebellum: convergent evidence from task and seed-based resting-state fMRI analyses in a single large cohort. NeuroImage. 2018;172:437–49.
24. Guell X, Schmahmann JD, Gabrieli JD, Ghosh SS. Functional gradients of the cerebellum. Elife. 2018;7:e36652.
25. Schmahmann JD, Guell X, Stoodley CJ, Halko MA. The theory and neuroscience of cerebellar cognition. Annu Rev Neurosci. 2019;42:337–64.
26. Clark SV, Semmel ES, Aleksonis HA, Steinberg SN, King TZ. Cerebellar-Subcortical-Cortical systems as modulators of cognitive functions. Neuropsychol Rev. 2021;31:422–46.
27. Henriques RN, Rokem A, Garyfallidis E, St-Jean S, Peterson ET, Correia MM. [Re] optimization of a free water elimination two-compartment model for diffusion tensor imaging. 2017.
28. Zhang H, Schneider T, Wheeler-Kingshott CA, Alexander DC. NODDI: practical in vivo neurite orientation dispersion and density imaging of the human brain. NeuroImage. 2012;61:1000–16.
29. Kroenke K, Spitzer RL, Williams JBW. The PHQ-9: validity of a brief depression severity measure. J Gen Intern Med. 2001;16:606–13.
30. Spitzer RL, Kroenke K, Williams JBW, Löwe B. A brief measure for assessing generalized anxiety disorder: the GAD-7. Arch Intern Med. 2006;166:1092.
31. Hamilton M, THE ASSESSMENT OF ANXIETY, STATES BY RATING. Br J Med Psychol. 1959;32:50–5.
32. Hamilton M, A RATING SCALE FOR, DEPRESSION. J Neurol Neurosurg Psychiatry. 1960;23:56–62.
33. Folstein MF, Folstein SE, McHugh PR. Mini-mental state. J Psychiatr Res. 1975;12:189–98.
34. Pasternak O, Sochen N, Gur Y, Intrator N, Assaf Y. Free water elimination and mapping from diffusion MRI. Magn Reson Med. 2009;62:717–30.
35. Garyfallidis E, Brett M, Amirbekian B, Rokem A, Van Der Walt S, Descoteaux M et al. Dipy, a library for the analysis of diffusion MRI data. Front Neuroinform. 2014;8.
36. Le Bihan D, editor. Diffusion and perfusion magnetic resonance imaging: applications to functional MRI. New York: Raven; 1995.
37. Daducci A, Canales-Rodríguez EJ, Zhang H, Dyrby TB, Alexander DC, Thiran J-P. Accelerated microstructure imaging via convex optimization (AMICO) from diffusion MRI data. NeuroImage. 2015;105:32–44.
38. Diedrichsen J, Balsters JH, Flavell J, Cussans E, Ramnani N. A probabilistic MR atlas of the human cerebellum. NeuroImage. 2009;46:39–46.
39. Diedrichsen J, Maderwald S, Küper M, Thürling M, Rabe K, Gizewski ER, et al. Imaging the deep cerebellar nuclei: A probabilistic atlas and normalization procedure. NeuroImage. 2011;54:1786–94.
40. Hua K, Zhang J, Wakana S, Jiang H, Li X, Reich DS, et al. Tract probability maps in stereotaxic spaces: analyses of white matter anatomy and tract-specific quantification. NeuroImage. 2008;39:336–47.
41. Oishi K, editor. MRI atlas of human white matter. 2 ed. London: Academic; 2011.

42. Wakana S, Caprihan A, Panzenboeck MM, Fallon JH, Perry M, Gollub RL, et al. Reproducibility of quantitative tractography methods applied to cerebral white matter. NeuroImage. 2007;36:630–44.
43. Moreno-Rius J. The cerebellum under stress. Front Neuroendocr. 2019;54:100774.
44. Collier Q, Veraart J, Jeurissen B, Vanhevel F, Pullens P, Parizel PM, et al. Diffusion kurtosis imaging with free water elimination: A bayesian Estimation approach. Magn Reson Med. 2018;80:802–13.
45. Ju Y, Ou W, Su J, Averill CL, Liu J, Wang M, et al. White matter microstructural alterations in posttraumatic stress disorder: an ROI and whole-brain based meta-analysis. J Affect Disord. 2020;266:655–70.
46. Suo X, Lei D, Li W, Chen F, Niu R, Kuang W, et al. Large-scale white matter network reorganization in posttraumatic stress disorder. Hum Brain Mapp. 2019;40:4801–12.
47. Andica C, Kamagata K, Hatano T, Saito Y, Ogaki K, Hattori N, et al. MR biomarkers of degenerative brain disorders derived from diffusion imaging. J Magn Reson Imaging. 2020;52:1620–36.
48. Genc S, Malpas CB, Holland SK, Beare R, Silk TJ. Neurite density index is sensitive to age related differences in the developing brain. NeuroImage. 2017;148:373–80.
49. Kamiya K, Hori M, Aoki S. NODDI in clinical research. J Neurosci Methods. 2020;346:108908.
50. Kitamura S, Matsuoka K, Takahashi M, Yoshikawa H, Minami A, Ohnishi H, et al. Association of adverse childhood experiences and cortical neurite density alterations with posttraumatic stress disorder symptoms in autism spectrum disorder. Front Psychiatry. 2023;14:1215429.
51. Van Overwalle F, Ma Q, Heleven E. The posterior Crus II cerebellum is specialized for social mentalizing and emotional self-experiences: a meta-analysis. Soc Cognit Affect Neurosci. 2020;15:905–28.
52. Laidi C, Hajek T, Spaniel F, Kolenic M, d'Albis M-A, Sarrazin S, et al. Cerebellar parcellation in schizophrenia and bipolar disorder. Acta Psychiatr Scand. 2019;140:468–76.
53. Ernst TM, Brol AE, Gratz M, Ritter C, Bingel U, Schlamann M, et al. The cerebellum is involved in processing of predictions and prediction errors in a fear conditioning paradigm. eLife. 2019;8:e46831.

Publisher's note